Epistasis at the SARS-CoV-2 RBD Interface and the Propitiously Boring Implications for Vaccine Escape

Nash D. Rochman[1*], Guilhem Faure[2], Yuri I. Wolf[1], Peter L. Freddolino[3,4], Feng Zhang[2,5,6,7,8*], and Eugene V. Koonin[1*]

[1]National Center for Biotechnology Information, National Library of Medicine, Bethesda, MD 20894 [2]Broad Institute of MIT and Harvard, Cambridge, MA 02142; [3]Department of Biological Chemistry, University of Michigan Medical School, Ann Arbor, MI, USA; [4]Department of Computational Medicine and Bioinformatics, University of Michigan Medical School, Ann Arbor, MI, USA; [5]Howard Hughes Medical Institute, Massachusetts Institute of Technology, Cambridge, MA 02139; [6]McGovern Institute for Brain Research, Massachusetts Institute of Technology, Cambridge, MA 02139; [7]Department of Brain and Cognitive Sciences, Massachusetts Institute of Technology, Cambridge, MA 02139; and [8]Department of Biological Engineering, Massachusetts Institute of Technology, Cambridge, MA 02139

[*]For correspondence: nash.rochman@nih.gov, zhang@broadinstitute.org, koonin@ncbi.nlm.nih.gov

Keywords: SARS-CoV-2, Delta Variant, Gamma Variant, Omicron Variant, Escape Mutants, Epistasis, Protein Structure Modelling, Rosetta

Abstract

At the time of this writing, December 2021, potential emergence of vaccine escape variants of severe acute respiratory syndrome coronavirus 2 (SARS-CoV-2) is a grave global concern. The interface between the receptor-binding domain (RBD) of SARS-CoV-2 spike (S) protein and the host receptor (ACE2) overlap with the binding site of principal neutralizing antibodies (NAb), limiting the repertoire of viable mutations. Nonetheless, variants with multiple mutations in the RBD have rose to dominance. Non-additive, epistatic relationships among RBD mutations are apparent, and assessing the impact of such epistasis on the mutational landscape is crucial. Epistasis can substantially increase the risk of vaccine escape and cannot be completely characterized through the study of the wild type (WT) alone. We employed protein structure modeling using Rosetta to compare the effects of all single mutants at the RBD-NAb and RBD-ACE2 interfaces for the WT, Delta, Gamma, and Omicron variants. Overall, epistasis at the RBD interface appears to be limited and the effects of most multiple mutations are additive. Epistasis at the Delta variant interface weakly stabilizes NAb interaction relative to ACE2 interaction, whereas in the Gamma variant, epistasis more substantially destabilizes NAb interaction. Although a small, systematic trend towards NAb destabilization not observed for Delta or Gamma was detected for Omicron, and despite bearing significantly more RBD mutations, the epistatic landscape of the Omicron variant closely resembles that of Gamma. These results suggest that, although Omicron poses new risks not observed with Delta, structural constraints on the RBD hamper continued evolution towards more complete vaccine escape. The modest ensemble of mutations relative to the WT that are currently known to reduce vaccine efficacy is likely to comprise the majority of all possible escape mutations for future variants, predicting continued efficacy of the existing vaccines.

Significance

Emergence of vaccine escape variants of SARS-CoV-2 is arguably the most pressing problem during the COVID-19 pandemic as vaccines are distributed worldwide. We employed a computational approach to assess the risk of antibody escape resulting from mutations in the receptor-binding domain of the spike protein of the wild type

SARS-CoV-2 virus as well as the Delta, Gamma, and Omicron variants. At the time of writing, December, 2021, Omicron is poised to replace Delta as the dominant variant worldwide. The efficacy of the existing vaccines against Omicron could be substantially reduced relative to the WT and the potential for vaccine escape is of grave concern. Our results suggest that although Omicron poses new evolutionary risks not observed for the Delta variant, structural constraints on the RBD make continued evolution towards more complete vaccine escape unlikely. The modest set of escape-enhancing mutations already identified for the wild type likely include the majority of all possible mutations with this effect.

Introduction

When severe acute respiratory syndrome coronavirus 2 (SARS-CoV-2), first emerged as a global public health concern early in 2020, there was considerable debate regarding whether the low mutation rate of the virus and the relatively inflexible receptor-binding domain (RBD) of the antigenic spike (S) protein would admit robust host adaptation(1, 2). By 2021, it became clear that SARS-CoV-2 has access to a broad mutational repertoire enabling extensive diversification(3) and that without vaccination, SARS-CoV-2 would likely result in substantial global disease burden for a protracted period(4, 5). The development of multiple, effective vaccines against SARS-CoV-2(6) make it possible to dramatically reduce this burden. However, at the time of writing, December, 2021, the majority of the global population remains unvaccinated as the Omicron variant is poised to replace the Delta variant as the dominant strain worldwide. Existing vaccine efficacy against the Omicron variant might be substantially reduced relative to the WT https://www.cdc.gov/coronavirus/2019-ncov/science/science-briefs/scientific-brief-omicron-variant.html, and the potential for continued evolution towards more complete vaccine escape(7) is a major global concern https://www.cdc.gov/coronavirus/2019-ncov/variants/variant-info.html.

The interface between the receptor-binding domain (RBD) of the S protein and the host receptor (ACE2) largely overlaps with the binding sites for the most potent neutralizing antibodies (NAb)(8, 9), limiting the scope of viable mutations. Nevertheless, multiple variants containing single mutations in the RBD that, to different extents, reduce NAb binding have begun to circulate(8-10). Moreover, variants with multiple mutations in the RBD have risen to dominance outcompeting the wild type (WT, identical to Wuhan-Hu-1) and single mutants (see below). These dynamics could result from non-additive, epistatic interactions among the mutated sites(10, 11) or simply from additive effects of multiple mutations(11). The effects of all single mutations in the RBD relative to the WT have been studied, and several mutations producing partial antibody escape have been identified (8, 12). Epistasis among RBD mutations has the potential to substantially increase the risk of escape variant emergence and cannot be characterized through the study of the WT alone.

Using the Rosetta software suite https://rosettacommons.org(13), we estimated and compared the effects of all single non-synonymous mutants at the RBD-NAb and RBD-ACE2 interfaces for the WT as well as Delta (452R, 478K), Gamma (417T, 484K, 501Y), and Omicron (339D, 371L, 373P, 375F, 417N, 440K, 446S, 477N, 478K, 484A, 493R, 496S, 498R, 501Y, 505H) variants. The Delta and Gamma variants were dominant in different regions of the world with rising frequencies as of Summer, 2021(14, 15). Delta rose to global dominance in the following months and, at the time of writing, Omicron is rapidly growing in frequency and is expected to become the next globally dominant strain. We establish the distribution of RBD mutations on the plane bounded by the costs of ACE2 and NAb binding and classify the direction and magnitude of epistatic interactions between variant mutations and the broader mutational repertoire. The results reveal only weak epistasis which, although more pronounced for the Gamma and Omicron variants than for the Delta variant, suggests limited potential for continued evolution towards more complete vaccine escape.

Results

Rationale

Epistatic interactions among mutations in the RBD of SARS-CoV-2 S protein are of interest and concern because they might substantially increase the risk of vaccine escape. Mutations in the RBD subtly change the shapes of the interfaces between RBD and ACE2, and between RBD and NAb (Figure 1A). While the structure of the WT RBD-ACE2 interface is highly similar to that of the RBD-NAb interface (see below), a single mutation in the RBD can result in distinct shape changes in both interfaces. These changes can be depicted by the position of each mutant on the plane bounded by the receptor binding cost and the antibody cost (Figure 1B). The cost is the increase (positive cost) or decrease (negative cost) in the ACE2 or NAb binding affinity relative to the WT. The four quadrants of this plane (Figure 1B) represent four broad categories of mutations. Mutations in the top, right quadrant are strongly destabilizing relative to both

ACE2 and the NAb. The bottom, right quadrant contains mutants that strongly destabilize the interaction with ACE2 but not with the NAb. Most mutants in these quadrants are not evolutionarily viable. Mutants in the bottom, left quadrant stabilize or only weakly destabilize both interfaces. These mutations may or may not provide a selective advantage to the virus depending on the fraction of the host population that has been vaccinated or has recovered from prior infection. The top, left quadrant contains mutations that strongly destabilize the interaction with NAb but not with ACE2 and therefore are most likely to admit vaccine escape.

Single-mutant vaccine escape candidates for the wild type RBD

Starting with the two crystal structures of interest, the RBD in complex with ACE2 https://www.rcsb.org/structure/6M0J(16) and the RBD in complex with the NAb CV30, https://www.rcsb.org/structure/6XE1, we generated a representative ensemble of 50 native conformations per complex following standard Rosetta protocols (see Methods and Discussion for details). Although NAb that bind epitopes, which do not overlap with the RBD have been identified(8), at the time of writing, the antibodies most critical for assessing the risk of vaccine escape appear to overlap with the RBD(9) and are well represented by CV30. Regions important for antibody binding are known to overlap broadly among human coronaviruses(17). We then identified the RBD residues at the interface for each conformation and, in all conformations, introduced all single amino acid substitutions at these sites. For the WT and Delta variant, 52 residues (Table 1) were identified at the interface of at least one conformation for either complex. Four additional residues were identified for the Gamma and/or Omicron variants. Sites 480 and 488 are connected by a disulfide bond and were found to be unsuitable for substitution.

All 19 substitutions in each of the remaining 54 sites were investigated, with the exception of WT reversion for the variants. Note that substitutions made in the WT are all single mutants; those in the Delta variant are triple mutants (given that this variant contains two mutations in the RBD); those in the Gamma variant are quadruple mutants; and those in the Omicron variant each encompass 16 mutations in total. We

chose to examine all variants containing Delta/Gamma/Omicron substitutions and an additional substitution at the interface rather than probing a randomly selected, representative ensemble of multiple mutants relative to the WT because the mutations present in the Delta/Gamma/Omicron variants are known to be of biological and epidemiological relevance and the space of all such multiple mutants is prohibitively large. Altogether, this analysis produced more than 400k structures which necessitated the development of a computationally efficient, and therefore simplified, protocol. To address this need, mutants were introduced into each conformation without repacking of adjacent sidechains or backbone minimization. This minimalist approach yielded favorable comparisons to the available experimental data (see below). However, generally, substitutions might introduce steric or charge clashes within the conformations in which the mutations were introduced (without repacking and minimization). Inference of the relative change in binding affinity for the ACE2 and NAb complexes is limited for such mutations. However, we observed a favorable comparison to experimental data in this respect as well, whereby few experimentally predicted escape mutations (relative to the WT) fall into this, inference-limited, category (see below).

Structure stability was estimated by the total score, *S*, in arbitrary units produced by the empirically-driven Rosetta Energy Function 2015(18) (labelled REU for "Rosetta Energy Units", https://new.rosettacommons.org/docs/latest/rosetta_basics/Units-in-Rosetta). The total score was calculated for each of the 50 conformations of the NAb and ACE2 complexes generated, and the mean value was assessed with, S_M^C, and without, S_{WT}^C, the mutation. The receptor cost and antibody cost were estimated as $[S_M^C - S_{WT}^C]_{ACE2}$ and $[S_M^C - S_{WT}^C]_{NAb}$, respectively. The interface free energy (ΔG) was also more directly approximated by the difference between the total score of the unbound state and the complex, $S^C - S^U$. The effect of the mutation on this value ($\Delta\Delta G$) was reported for both complexes, $(S_M^C - S_M^U) - (S_{WT}^C - S_{WT}^U)$. Figure 1C shows the distribution of RBD mutations on the plane bounded by the ACE2 and NAb binding costs and putative NAb escape candidates, for which $[S_M^C - S_{WT}^C]_{NAb} - [S_M^C - S_{WT}^C]_{ACE2} > 1$ or $\Delta\Delta G_{NAb}$-$\Delta\Delta G_{ACE2}$>1 and $[S_M^C - S_{WT}^C]_{ACE2} < 13$. The threshold value of 13 was selected to remove from

consideration mutations that likely produce steric or charge clashes in the structure; few experimentally validated escape candidates were observed above this value (see below).

Mutants showed strong clustering along the diagonal (identity line: receptor cost is equal to antibody cost), indicating that most mutations similarly affected the WT RBD-ACE2 and RBD-NAb complexes. Mutations in the top, left quadrant of the plane, which corresponds to strong destabilization of the interaction with NAb but not with ACE2, are the strongest candidates for vaccine escape, followed by those in the bottom, left quadrant, which includes weakly destabilizing mutations. The selective advantage (or lack thereof) of mutations in this quadrant depends on the fraction of the host population that has been vaccinated or has recovered from prior infection (see Discussion). In a fully vaccinated population, mutations that substantially reduce infectivity through the destabilization of receptor binding, while also destabilizing the interaction with NAb, could still provide a selective advantage. In particular, multiple mutations in 6 sites (417, 477, 484, 491, 493, 499) were found to substantially destabilize the RBD-NAb complex relative to the RBD-ACE2 complex (Figure S1). Additionally, we identified site 453 to harbor mutations that simultaneously stabilize the RBD-ACE2 complex and destabilize the RBD-NAb complex. These observations are broadly consistent with the results of deep mutational scanning(8, 9, 19-22). Therefore, we conservatively considered all mutations, for which the antibody cost exceeded the receptor cost, to be viable escape candidates.

Single-mutant vaccine escape candidates for the Gamma, Delta, and Omicron variant RBDs and predicted epistatic interactions

Having charted the ACE2-binding and NAb-binding landscapes for the WT RBD, we sought to identify the most prominent combinations of RBD mutations circulating over the course of the pandemic. As of June, 16th, 2021, there were 53 countries, from which more than 1,000 SARS-CoV-2 isolates were contributed to the GISAID(23) database (see Data Availability). For each of these locations, we randomly selected 1,000 isolates and reported the frequency of each combination of RBD mutations among the 53,000

218 selected isolates over time. Figure 2A displays this region-normalized global prevalence
219 of the 10 most common combinations of RBD mutations. The 6 RBD single-mutants
220 (501Y/Alpha Variant, 477N, 439K, 484K, 478K, and 459F) began emerging between
221 July and November 2020. All these single mutants were eventually displaced by 4 RBD
222 multiple mutants (452R|478K/Delta Variant, 417T|484K|501Y/Gamma Variant,
223 417N|484K|501Y/Beta Variant, and 346K|484K|501Y), which began emerging in
224 November, 2020, with the exception of Beta, which according to our analysis, first
225 appeared in July. By March, 2021, the WT had become less prevalent than the Alpha,
226 Gamma, and Delta variants. We pursued further analysis for the Delta, Gamma, and the
227 recently identified Omicron variant RBDs given their high and rising global prevalence.
228 The complexes were prepared starting from the WT crystal structures and treated
229 identically to the WT. We also discuss how similar results may be obtained starting
230 directly with the native conformations approximated for the WT, substantially reducing
231 the computational burden (see Methods).
232
233 The rapid emergence and subsequent displacement of RBD single mutants might in
234 part result from epistasis among the RBD variant residues or could be due to purely
235 additive interactions. The most prominent trend was the displacement of the single
236 mutant, 501Y (Alpha variant) by the Beta and Gamma variants (both also containing
237 501Y). Residue 501Y has been shown to substantially increase the binding affinity with
238 ACE2 which, however, is reduced with the addition of mutation 417N in the Beta
239 variant(11). In contrast, 417N severely reduces the neutralizing activity of a variety of
240 NAb(24). These observations imply that mutations in site 417 provide a selective
241 advantage through destabilization of the NAb complex, but given the large overlap
242 between the RBD-NAb and RBD-ACE2 interfaces, maintenance of sufficient infectivity
243 requires a compensatory mutation, such as 501Y, that stabilizes the RBD-ACE2
244 complex. Note that the emergence of these variants preceded widespread vaccination
245 and that, although the competition between antibody and receptor binding is present
246 even during an infection of a naïve host, evolutionary pressures are likely to shift with
247 increasing rates of vaccination and prior infection (see below). At the time of writing, the
248 origin of the Omicron variant , and thus the evolutionary pressures that led to its

emergence remain unknown (see discussion); however, despite bearing many more RBD mutations, the epistatic landscape at the interface is highly similar between the Gamma and Omicron variants (see below).

Examination of the interface footprints, defined as the ensemble of sites predicted to lie at the interface of at least one of the 50 conformations for each complex, for the 8 complexes of interest, demonstrates that the RBD makes a greater number of contacts with NAb than with ACE2 within the same range of sites, 403-506 (Figure 2B). The footprints of the WT and Delta variant interfaces in both the RBD-ACE2 and the RBD-NAb complexes are identical. The WT/Delta RBD-ACE2 footprint consists of 37 sites whereas the WT/Delta RBD-NAb footprint includes 51 sites (Table 1). The Gamma RBD-ACE2 footprint consists of 41 sites including all those in the WT/Delta footprint, with the single exception of site 484, and five additional sites. The Gamma RBD-NAb footprint consists of 53 sites including all those in the WT/Delta interface and, in addition, sites 408 and 480. The Omicron RBD-ACE2 footprint consists of 37 sites with three WT sites missing (including 484) and three additions. The Omicron RBD-NAb footprint includes 50 sites with one WT site missing.

Sites in the RBD-NAb footprint that are not shared by the RBD-ACE2 footprint might provide routes for the emergence of vaccine escape variants. However, because the RBD-ACE2 footprint is smaller than the RBD-NAb interface, the former is more sensitive to perturbation than the latter, for example, from mutations in site 417, which is part of the footprint of all 8 complexes. Notably, site 484 is absent from the Gamma and Omicron RBD-ACE2 footprints, but remains in the respective RBD-NAb footprints. Also of note, site 446, which is mutated in Omicron, is present in the RBD-NAb footprint but not the RBD-ACE2 footprint for this variant. Consistent with the differences in the footprints, we found the Omicron and, to a lesser extent, Gamma variant RBD conformations in complex with ACE2 to be significantly different from that of the WT and Delta variants, which could not be differentiated from one another. All variant RBD conformations in complex with the NAb were found to be significantly different from that of the WT. For Delta and Gamma, this difference was modest and smaller in magnitude

than the variability among the RBD-NAb conformations, whereas Omicron showed a more pronounced difference from the WT (Figure 2C).

Classical multidimensional scaling (CMDS) applied to the pairwise interface RMSDs among all RBD-ACE2 and RBD-NAb complexes showed that the Gamma and Omicron RBD-ACE2 structures lie on a shared continuum of conformational change relative to the WT, with the Omicron conformations being closer to Gamma than to the WT. In contrast, Omicron, Gamma, and to a lesser extent, Delta RBD-NAb structures all represent distinct conformational changes relative to the WT (Figures 2D and S2). Despite these differences, the effects of mutations in the RBD were found to be principally additive in all variants, that is, there seems to be little epistasis.

When a second mutation, M_j, is introduced in addition to a prior mutation, M_i (Figure 3A), the resulting conformational change can be additive so that the effect of the two mutations is the sum of the effects of the two individual mutations. In this case, the position of the double-mutant $M_{i,j}$ on the plane defined by the receptor cost and antibody cost relative to the single mutant, M_i, will be the same as that of the single-mutant, M_j, relative to the WT. If the conformational change is non-additive, representing an epistatic relationship, the resulting trends can be classified by their impact on potential vaccine escape. Such trends could be escape-neutral when the ensemble of candidate vaccine escape mutations differs from that for the WT, but the number of such candidates is the same; escape-minimizing when the antibody cost is on average reduced relative to the receptor cost across all mutations for the mutant vs the WT; or escape-exacerbating where the antibody cost is on average increased.

The landscape of mutants predicted to enhance vaccine escape for the Delta variant was almost identical to that of the WT but differed significantly from the Gamma and Omicron landscapes (Figure 3B). These trends are summarized in Table 2, which tabulates all non-shared candidates. There are 15(13) escape candidates in the WT that were not predicted to enhance escape for Delta and 6(2) candidates in Delta but not WT (values in parentheses are mutations with $[S_M^C - S_{WT}^C]_{ACE2} < 13$, regardless of whether

311 or not the mutation is a candidate, a threshold chosen to mitigate potential artifacts
312 caused by steric or charge clashes). In contrast, in the case of Gamma, there were
313 32(28) candidates identified in WT but not Gamma, and 86(66) candidates identified in
314 Gamma but not the WT. Omicron demonstrated intermediate behavior with 67(59)
315 candidates identified in WT but not Omicron, and 75(48) candidates identified in
316 Omicron but not the WT. Thus, we identified 9(11) fewer escape candidates for Delta
317 compared to the WT, but 54(38) additional candidates for Gamma, and either 8
318 additional candidates or 11 fewer candidates (ignoring potential steric/charge clashes in
319 the WT) for Omicron.
320
321 Consistent with the more dramatic conformational change observed in the RBD-ACE2
322 complex relative to the RBD-NAb complex, the non-additive effects observed in the
323 Gamma variant appear to predominantly result from the decreased sensitivity of the
324 RBD-ACE2 interface to mutation. This conclusion is compatible with the available
325 experimental results. Figure S3 shows the distribution of the receptor cost, $[S_M^C -$
326 $S_{WT}^C]_{ACE2}$, for two categories of mutations and for each of the three receptor complexes:
327 those at the interface that have been experimentally demonstrated to reduce
328 neutralizing activity of antibodies COV2-2050 and COV2-2479 in the WT(8), and all
329 others (included in the same experimental study) at the interface. As discussed above,
330 the upper bound for the receptor cost, $[S_M^C - S_{WT}^C]_{ACE2}$, is lower for mutations predicted
331 to reduce NAb activity than for other mutations. However, the Gamma candidate
332 ensemble exhibits a reduced median receptor cost. In other words, in the Gamma
333 variant, mutations that are predicted to reduce NAb activity are also less likely than
334 other mutations to reduce the receptor binding affinity relative to the WT and Delta
335 variant. The three residues within the RBD-ACE2 footprint of the Omicron variant not
336 present in the WT overlap with those of the Gamma variant (404, 439, and 499) and,
337 although not statistically significant, the decreased cost of receptor binding was
338 observed for Omicron as well. The Omicron variant additionally displayed a modest
339 reduction in median receptor cost for the broader category of experimentally studied
340 mutations, suggesting greater flexibility at the receptor interface (Figure S3).
341

342 Figure 4 summarizes the magnitude of the increased risk of vaccine-escape for each
343 mutation at the RBD interface (given $[S_M^C - S_{WT}^C]_{ACE2} < 13$) for each variant relative to
344 the WT. Epistasis increasing the risk of vaccine-escape is primarily apparent in three
345 regions of the RBD interface: site 417, site 477, and site 494 together with the
346 surrounding neighborhood. The trend in site 417 was observed only in the Gamma and
347 Omicron variants, which already contain mutations at that site, showing that further
348 changes to this site could result in enhanced vaccine escape. However, the
349 epidemiological implications of this finding are limited considering that mutations in site
350 417 are likely to pose a risk of vaccine escape in most variants. The enhanced escape
351 associated with mutations in site 477 for all variants relative to the WT, together with the
352 early spread of 477N and the presence of 477N in the Omicron variant, suggest that this
353 site could play an important role in host adaptation. Most prominently, mutations in site
354 494 and the surrounding neighborhood are likely to enhance vaccine escape in all
355 variants. Indeed, 494P has both been found in circulation and experimentally
356 demonstrated to reduce antibody neutralization capacity of convalescent sera(25).
357
358 In addition to these apparent differences among the ensembles of candidate vaccine-
359 escape mutations, we observed sites that harbored no candidates, but nevertheless
360 displayed signatures of increased risk of vaccine escape for Gamma and/or Omicron.
361 The two most notable trends were observed in sites 408 and 504 (Figure S4). All but
362 one substitution in site 408 enhance vaccine-escape for Gamma and Omicron, but
363 surprisingly, all have the opposite effect in Delta. Similarly, all substitutions at site 504
364 substantially enhance vaccine-escape in Gamma and Omicron but exert a modest
365 opposite effect in Delta. However, these mutations are not considered candidates in our
366 analysis because, even for Gamma and Omicron, they destabilize the ACE2 interaction
367 to a greater extent than the interaction with NAb. Additionally, $[S_M^C - S_{WT}^C]_{ACE2} \gg 13$ for
368 substitutions at site 504, which limits confidence in the assessment of trends at this site.
369
370 Importantly, few differences were observed between the epistatic landscapes of the
371 Gamma and Omicron variants, mainly in sites 417, 439, 499 (see Figure 4), and 446
372 (see Figure S4). Sites 417 (reduced escape-related epistasis) and 446 (increased

373 escape-related epistasis) are already mutated in Omicron and the signatures in sites
374 439 and 499 are modest relative to the consistent trend observed in site 494.
375 Nonetheless, it is important to acknowledge a small, systematic bias towards NAb
376 destabilization within the Omicron variant that is not observed within Gamma or Delta
377 (Figure 4, inset and Figure S5). As demonstrated above, unlike the RBD-ACE2
378 complex, which displays a shared continuum of conformational change relative to the
379 WT, RBD-NAb structures all represent distinct conformational changes (Figures 2D and
380 S2) with the greatest change observed for Omicron. Most mutations, which modestly
381 destabilize the WT RBD-NAb complex ($[S_M^C - S_{WT}^C]_{NAb} < 10$), are slightly more
382 destabilizing in the Omicron RBD-NAb complex compared to the other variants. As
383 discussed above, only a subset of these mutations are considered candidates for
384 antibody escape, which depends on the properties of the mutation within the RBD-
385 ACE2 complex as well. The principal escape signatures are conserved between the
386 Gamma and Omicron variants, with fewer escape candidates identified overall for the
387 Omicron variant. However, this systematic destabilization of the Omicron RBD-NAb
388 complex suggests, in principle, additional avenues towards vaccine escape.
389

390 ## Discussion

391 Here we report the results of a computational study predicting the effects of all single
392 mutants at the RBD-NAb and RBD-ACE2 interfaces for the WT as well as the Delta,
393 Gamma, and Omicron variants of SARS-CoV-2 on receptor and antibody binding. For
394 the WT, we found multiple mutations in 6 sites (417, 477, 484, 491, 493, 499) that are
395 predicted to significantly destabilize the RBD-NAb complex relative to the RBD-ACE2
396 complex and appear to pose a risk of vaccine escape, which is broadly consistent with
397 the results of deep mutational scanning(8, 9, 19-22). Overall, most mutations at the
398 interface were found to similarly effect the WT and all variants, indicating limited
399 epistasis at the interface. Non-additive, epistatic interactions predicted to increase the
400 risk of vaccine-escape were apparent, however, at sites 477 and 494 as well as in the
401 surrounding neighborhood. This trend is particularly prominent in the Gamma variant so
402 that, across all sites at the interface, we predicted 22% more escape candidate
403 mutations for the Gamma variant than for the WT. In contrast, there is little apparent

404 epistasis in the Delta variant, and across all sites at the interface, we predicted 4%
405 fewer candidate mutations compared to WT. Despite harboring many more RBD
406 mutations and displaying a small, systematic trend towards NAb complex
407 destabilization, the Omicron variant demonstrated intermediate behavior with only 3%
408 more candidate escape mutations compared to the WT.
409
410 Epistasis is a major if not the principal driver of protein evolution(26). Compensatory
411 mutations are particularly strong epistatic interactions that can result in
412 chemotherapeutic(27) or antimicrobial(28) drug resistance, and are commonly observed
413 throughout species evolution(29). In a completely susceptible population, mutation
414 501Y, which appears to substantially increase infectivity(11), is expected to evolve
415 under positive selection. As a population gains immunity, through prior exposure and/or
416 vaccination, selective pressures rapidly change to promote the emergence of resistant
417 variants(7). Under these conditions, 501Y and other mutations, which increase
418 infectivity might primarily play the role of compensators for mutations destabilizing NAb
419 interactions, such as 417N or 417T. As global vaccinations rise, due to changing
420 evolutionary pressures, it can be expected that more mutations emerge that destabilize
421 the interactions of the RBD with both NAb and ACE2, thus resulting in (partial) escape
422 variants that, however, also have reduced infectivity. However, variants such as
423 Gamma that carry both an antibody destabilizing mutation and a compensatory
424 mutation have the potential to undercut this trend.
425
426 At the time of writing, the origins of the Omicron variant are unclear and is suspected to
427 have evolved over an extended period of time within an immunocompromised
428 individual(s) or an animal reservoir(30). Such environments could present selective
429 pressures distinct from the broader human host population, but the changing
430 competition between receptor and antibody binding described above is likely to be
431 conserved. Despite the more pronounced conformational change, the average behavior
432 of the conformational ensemble selected to represent the Omicron variant was found to
433 be less destabilizing for the receptor compared to Gamma but highly destabilizing for

434 the antibody, indicating that our model for Omicron is likely to be at least as accurate if
435 not more accurate than those for the Gamma and Delta variants (Figures S12-13).
436
437 Above all else, we find it important to highlight three points. 1) The epistatic landscapes
438 of the Gamma and Omicron variants are highly similar (Figure 4). 2) We find fewer, not
439 more, escape-exacerbating mutations in Omicron compared to Gamma (Table 2). 3)
440 These features persist in spite of the fact that RBD-ACE2 structures represent a shared
441 continuum of conformational change relative to the WT, with the Omicron conformations
442 being closer to Gamma than the WT (Figures 2D and S2), indicating that the magnitude
443 of conformational change does not trivially correlate with the propensity for exacerbated
444 antibody escape. The neutralizing activity of existing vaccine elicited NAb against the
445 Omicron variant is likely to be substantially reduced(31), but multi-dose vaccination is
446 expected to recover efficacy(32). Our results emphasize that, although the adaptive
447 repertoire of SARS-CoV-2 may be robust, structural constraints on the RBD make
448 continued evolution towards more complete vaccine escape unlikely, suggesting
449 continued efficacy of the existing vaccines.
450
451 The work presented here is strictly computational, and although we demonstrate
452 agreement with experimental results where possible, many features not captured by the
453 models presented (involving protein expression, docking, and other factors) could
454 modulate antigen-receptor and/or antigen-antibody binding. Furthermore, although we
455 explore many conformations for both the RBD-ACE2 and RBD-NAb interfaces, we start
456 from a single crystal structure for each. We believe the conformational ensembles
457 selected to represent each complex are diverse enough to accurately reflect the relative
458 destabilization of the NAb and ACE2 complexes across the spectrum of RBD interface
459 mutations, which is the primary concern. However, this conformational diversity makes it
460 difficult to demonstrate stabilizing interactions, which are typically much weaker than
461 destabilizing ones(12). Although multiple low-energy conformations were resolved for all
462 variants and the WT, the average behavior of the conformational ensemble selected to
463 represent the Delta variant relative to the WT was found to be weakly destabilizing for
464 NAb and neutral for ACE2, whereas in the case of Gamma, it was weakly destabilizing

465 for both complexes. This is unlikely to accurately reflect the relative binding affinities
466 between these variants and the WT given the enhanced infectivity of both variants,
467 particularly Delta(14). However, it should be recognized that the relationship between
468 the measures of interface stability we report and viral life history traits (infectivity,
469 immune activity, etc.) is complex.
470
471 Although we believe we proposed sensible thresholds for determining which structures
472 can be analyzed with high confidence and the biological implications of the relative
473 destabilization of the NAb vs ACE2 are overt, the effects studied in this work do not
474 represent the entire diversity of possible host adaptation. It is incompletely understood
475 at the time of writing why the Delta variant appears to replicate faster than the WT(14)
476 and substitutions outside the Spike protein could play key roles in immune
477 modulation(33, 34). Even less is known about the Omicron variant. A targeted
478 exploration of the lowest-energy conformations achievable for each variant might yield
479 better agreement with the known properties of these variants and, in particular, reveal
480 stabilizing RBD-ACE2 interactions. However, this would likely come at the cost of
481 generalizability and decrease the power of our approach to predict relative
482 destabilization of interface mutations between NAb and ACE2 complexes.
483
484 We also emphasize that we limit our study to the RBD of the S protein. In principle,
485 epitopes located outside the RBD and far from the interface could play an important role
486 in the emergence of vaccine escape variants by decreasing the similarity between the
487 interaction with the antigen and receptor, and that between the antigen and an
488 antibody(35). However, if such effects were dominant, the satisfactory agreement
489 between our predictions, deep mutational scanning, and the observed frequency of
490 mutations within the RBD among the circulating variants, presumably, would not be
491 recovered. Nevertheless, many routes of adaptive evolution are potentially available to
492 this virus so that agreement with prior results is not a guarantee of predictive success.
493 Although we believe our results strongly suggest a limited repertoire of escape-
494 mediating mutations within the RBD, the possibility should be considered that mutations
495 outside the RBD have the potential to increase this repertoire.

496

497 Finally, we note that the space available for neutral evolution, even within the RBD
498 alone, is large. In principle, this makes possible the acquisition of many RBD mutations,
499 some combinations of which might exhibit substantially greater escape-exacerbating
500 epistatic effects than the variant substitutions explored in this work. However, this
501 appears unlikely considering the large number of mutations observed in the Omicron
502 variant, 15. We believe this variant is an excellent test case to probe the limits of
503 epistatic potential at the RBD interface.

504

505 **Conclusions**

506 We employed a computational approach to study the effects of all single mutations at
507 the RBD-NAb and RBD-ACE2 interfaces for the WT as well as the Delta, Gamma, and
508 Omicron variants of SARS-CoV-2. Overall, little epistasis at the RBD interface was
509 detected, with additive effects on the binding affinities observed for most pairs of
510 mutations. In the Delta variant, the observed non-additive trends weakly stabilize the
511 interaction of the RBD with the NAb relative to the interaction with ACE2, whereas in the
512 Gamma variant, epistasis is predicted to more substantially destabilize interaction with
513 the NAb relative to ACE2. The epistatic landscape of the Omicron variant closely
514 resembles that of Gamma, with an additional small systematic bias towards NAb
515 destabilization, but with fewer predicted escape candidates overall. These results
516 suggest that, although the Omicron variant poses new risks not observed for Delta,
517 including the evolution towards greater NAb destabilization, structural constraints on the
518 RBD make the continued evolution towards more complete antibody escape unlikely.
519 The modest ensemble of mutations relative to the WT that are currently known to
520 reduce vaccine efficacy is likely to comprise the majority of all possible escape
521 mutations for future variants, predicting continued efficacy of the existing vaccines.

522

523 ## Methods

524 **Selection of Crystal Structures**

525 In this work, we considered a single crystal structure of the SARS-CoV-2 spike protein
526 Receptor Binding Domain (RBD) in complex with the human receptor, Angiotensin
527 Converting Enzyme 2 (ACE2), PDB:6M0J(16). While there are likely multiple mutations

528 outside of the RBD which significantly affect binding characteristics of the spike protein,
529 as has been demonstrated for site 614(36), the structure of the RBD itself is unlikely to
530 be substantially modified by such mutations. Thus, while only able to reveal a subset of
531 mutations of interest, the focused study of RBD complexes presented here remains
532 biologically realistic.

533 Similarly, we consider a single crystal structure of the RBD in complex with a
534 neutralizing antibody (NAb),CV30 PDB:6XE1(37). CV30 was recognized early on as the
535 most potent NAb observed within the sera of a SARS-CoV-2 positive donor while the
536 majority of antibodies were found to target non-neutralizing epitopes outside of the
537 RBD(38). Subsequently, it became clear that antibodies targeting epitopes outside the
538 RBD, particularly those targeting the N-terminal domain (NTD), likely play a protective
539 role and mutations reducing the affinity of these antibodies may be epidemiologically
540 significant(35, 39). As acknowledged above regarding the selection of the spike crystal
541 structure, while our focus on CV30 is only able to reveal a subset of mutations of
542 interest, the mutations discussed in this work predicted to affect CV30 binding affinity
543 are likely highly epidemiologically relevant.

544

545 **Construction of Representative Ensembles of Interface Conformations**

546 Protein crystal structures may differ substantially from the native conformations(40).
547 Throughout this work, we utilize the Rosetta(13) software suite to approximate both wild
548 type (WT) and mutant conformations of the receptor and NAb complexes. All protocols
549 used throughout were implemented using the RosettaScripts(41) package and the XML
550 files used along with the associated executed command lines are made available in
551 Table S1. Approximation of the native conformational ensemble may be separated into
552 two steps, identifying the optimal side chain conformation (repacking) and moving the
553 protein backbone (minimization), to minimize the energy function applied. This may be
554 accomplished using the Rosetta Relax application which iteratively applies each of
555 these two steps.

556 Beginning with the crystal structure, we iteratively applied the FastRelaxMover using
557 default parameters (with the exception of disabling design) for up 12 iterations(15 for
558 Omicron) and up to 1000 repeats. We found the total score to be insensitive to
559 additional applications of FastRelax after 5 iterations on average. Each resulting
560 structure was scored using the InterfaceAnalyzerMover, repacking the unbound state
561 but not the bound state (as the input complex has already been optimized).

562 This protocol returns the total score, S, in arbitrary units produced by the empirically-
563 driven Rosetta Energy Function 2015(18) (labelled REU for “Rosetta Energy Units”,
564 https://new.rosettacommons.org/docs/latest/rosetta_basics/Units-in-Rosetta), as well as
565 dG separated which is the difference in the total score between the bound (complex)
566 and unbound state, S^C-S^U, derived from separating the binding partners. This protocol

567 may also be used to identify the residues within the complex which constitute the
568 interface.

569 Such an ensemble of structures often forms an “energy funnel”(42) where the root mean
570 square distance (RMSD) between superimposed backbone carbon atoms of each
571 structure and the structure with the lowest total score or the lowest dG separated is
572 positively correlated with the total score of that structure. In order to evaluate whether
573 such a funnel exists for these ensembles, we identified the structure with the lowest dG
574 separated and 90 residues predicted to be interface residues within the RBD in at least
575 one conformation in addition to the (+/-) 3 adjacent amino acid neighborhood of each
576 such residue (sites 400-424, 440-464, and 470-509 in the spike protein for WT;
577 additional sites 436-439 for Delta; additional sites 434-439 for Gamma; additional sites
578 434-439 and 510 for Omicron).

579 Figure S6 displays dG separated vs the interface RMSD for both complexes for the WT.
580 Few structures appear in the lower left corner of each plot from only one or two (NAb or
581 ACE2 respectively) independent “trajectories” of iterative FastRelax application
582 beginning with the crystal structure. Furthermore, while the lowest dG separated is more
583 than 30% greater in magnitude than the highest for both complexes, the interface
584 RMSD between any complex and the minimum dG separated complex is less than an
585 angstrom. These findings suggest selecting the single minimum dG separated
586 conformation for either complex is unlikely to constitute a realistic model of the native
587 interface and may in fact represent an unrealistic, entropically disfavored state(43).

588 Figures S7-9 display dG separated vs the interface RMSD for both complexes for the
589 Delta, Gamma, and Omicron variants. The distribution of conformations for the NAb is
590 similar to the WT for both Delta and Gamma; however, the minimum dG separated
591 obtained for Gamma is higher than that for the WT suggestive of antibody
592 destabilization for this variant. dG separated for Omicron is substantially higher
593 indicating significant destabilization. For Delta and Omicron, the distribution of
594 conformations for ACE2 more resembles a funnel suggestive of receptor stabilization for
595 these variants. For Gamma, there appear to be 2-3 distinct, equally low energy
596 conformations for ACE2 which makes the interpretation of the energy landscape more
597 challenging. For consistency, representative conformations were selected according to
598 the same protocol for all variants.

599 The construction of an ensemble of representative conformations is desired so that the
600 average behavior of such an ensemble is likely to reflect that of the native complex.
601 Ideally all available structures would be statistically weighted and included in this
602 ensemble; however, this is computationally intractable. Instead we selected 50
603 conformations for each complex as follows (see Figures S10-13): 1) The conformation
604 corresponding to the minimum total score after any iteration of FastRelax from each
605 independent “trajectory” beginning with the crystal structure was selected. 2) The 10
606 structures with the lowest total score were removed and the 10 structures with the
607 lowest dG separated were removed (these are not identical structures and as discussed

above, may represent unrealistic, entropically disfavored conformations). 3) The remaining structures were ranked by total score, r_S, and dG separated, r_G, and the 50 structures with the lowest composite rank, r_S+r_G, were selected. The PDB files for these structures are made available (see Data Availability). We believe the equally-weighted average behavior of these conformations, which are stable with well-resolved interfaces, constitute a reasonable model of the native complexes.

Analysis of Single Mutants Relative to WT, Delta, and Gamma

Given the 100 structures selected as described above (50 for each complex), a more restrictive list of 52 residues were predicted to lie at the interface of at least one structure for WT/Delta (spike protein sites 403-406,409,414-417,419-421,445-447, 449,453,455-461,473-478,484-498,500-506), 56 for Gamma (WT/Delta+408,439,480,499), and 53 for Omicron (WT/Delta+439,499,-445). We introduced all of the 19 possible mutations at each interface site (all 56 identified for any variant) for these 100 structures for the WT, Delta, Gamma, and Omicron variants with the exception of WT reversion for the variants. Mutations were introduced using the PackRotamersMover with design specified by the input resfile (see Data Availability for example). Only the targeted residue was modified: side chain conformations for all other residues were fixed and no backbone minimization was applied before filtering for candidates of interest as described below.

Introducing the mutation in this way without repacking and minimization results in many unrealistic, high-energy conformations which are difficult or impossible to interpret without further optimization. The benefit is speed. This procedure can be executed in under 30 seconds per structure while global repacking and minimization may take hours. An alternative approach is to apply backbone minimization and sidechain repacking within a local region of the structure centered at the modified site as implemented within Rosetta through the Flex ddG protocol(44). This approach has been used to accurately predict mutations conferring increased infectivity for SARS-CoV-2(45) and rationally design NAb against the antigen(46, 47) but is significantly slower than introducing mutations without, even local, optimization. With or without local optimization prior to filtering, global repacking and minimization may be desired to confirm top candidates. While our approach may introduce a higher false-negative rate than what one would achieve applying local optimization prior to filtering, it maximizes the breadth of candidate mutations considered and is able to recapitulate experimental results.

The total score and dG separated of the mutant structures were computed. Unlike in earlier steps where the unbound state was repacked during the dG separated calculation, no repacking was conducted for the reasons described above. Each mutant structure was matched with its initial WT/variant conformation and the change in dG separated, $(S_M^C-S_M^U)-(S_{WT}^C-S_{WT}^U)$, and total score, $S_M^C-S_{WT}^C$, were calculated. The average of each value taken over the ensemble of the 50 RBD-ACE2 conformations

was compared with experimentally determined ACE2 binding affinity for single RBD mutants(12). While the change in dG separated is technically the ddG for the mutant and may be expected to correspond to binding affinity, we find $(S_M^C-S_M^U)-(S_{WT}^C-S_{WT}^U)$ over this ensemble is not generally predictive of ACE2 affinity as $(S_M^C-S_M^U)-(S_{WT}^C-S_{WT}^U)$ is approximately zero for many mutants (Figure S14). This may be expected without repacking and minimization. Nonetheless, when nonzero, the change in dG separated compares favorably with ACE2 affinity (see below).

The change in total score is less sensitive and an adequate predictor of affinity (Figure S15) within the range $S_M^C-S_{WT}^C<5$ such that the minimum relative binding affinity decreases with increasing change in total score. Additional validation that $S_M^C-S_{WT}^C$ is a reasonable predictor of binding affinity, below some threshold, may be obtained through demonstrating $S_M^C-S_{WT}^C$ for each mutant is highly correlated between the RBD-ACE2 complex and the RBD-NAb complex. Furthermore, when the difference between the change in dG separated for the NAb complex and the dG separated for the ACE2 complex, $[(S_M^C-S_M^U)-(S_{WT}^C-S_{WT}^U)]_{NAb}-[(S_M^C-S_M^U)-(S_{WT}^C-S_{WT}^U)]_{ACE2}$, is positive, mutants lie above the identity line (y==x). The reverse is true for mutants falling below the identity line (Figures 1C/3B). In other words, on average, mutants in the RBD-ACE2 complex behave similarly to mutants in the RBD-NAb complex (which is what one would expect for realistic models of interfaces with an overlapping footprint). When differences do appear, they correspond to interactions with the RBD which are specific to the binding partner (ACE2/NAb) and are correctly reflected by the change in dG separated.

Directly Assessing Additive Effects Vs Epistasis

In the main text, we demonstrate that most mutations appear in a similar position of the receptor cost / antibody cost phase space for the WT and Gamma/Delta variants. Consequently, the ensemble of vaccine escape candidates is largely conserved. Whether epistatic effects due to multiple mutations are present or if the impact of multiple mutations is simply additive can be more directly assessed for each complex by plotting the change in the total score after introducing each mutation in the variant against the change in total score after introducing each mutation in the WT. Figure S5 displays the change in total score for each interface mutation relative to the WT and all variants for both ACE2 and the NAb. The minimum value (less 1) is subtracted from each distribution. The effect of each mutation at the interface in the WT is highly correlated for the Delta variant. This correlation is observed for the Gamma and Omicron variants as well with more significant variation as expected. There is additionally a small systematic bias towards greater NAb destabilization for mutations with small changes in the total score for the Omicron variant. As discussed in the main text, while this epistatic signature is not observed for the Gamma variant, this trend did not significantly alter the landscape of escape-exacerbating mutations.

Alternative Construction of Variant Ensembles

Beginning with the conformational ensemble constructed for the WT, we introduced the variant mutations 452R|478K for the Delta variant, 417T|484K|501Y for the Gamma variant, and 339D|371L|373P|375F|417N|440K|446S|477N|478K|484A|493R|496S|498R|501Y|505H for the Omicron variant and completed 5 rounds of the FastRelaxMover (15 for the Omicron variant) using default parameters (with the exception of disabling design) as described above. The resulting values for the total score and dG separated were comparable to that of the ensembles constructed for the variants beginning with the WT crystal structure (Figures S16-18); however, some structures displayed footprints more similar to the WT than those of the reference ensemble constructed as described in the main text. Thus, this computationally cheap alternative may be utilized for rapid evaluation; but the more comprehensive exploration of the conformational space described in the main is likely desired in many circumstances.

Data Availability

The data has been deposited through Zenodo(48) (https://doi.org/10.5281/zenodo.5297698) including GISAID acknowledgements. Previously published data were used for this work: GISAID(23). Data is additionally made available through FTP: https://ftp.ncbi.nih.gov/pub/wolf/_suppl/SARSstruct21/

Author contributions

NDR, and GF collected data; NDR, YIW, GF, PF, FZ, and EVK analyzed data; NDR and EVK wrote the manuscript that was edited and approved by all authors.

Acknowledgements

The authors thank the members of Jeff Gray's research group from Johns Hopkins University, in particular, Rahel Frick, for their consultation regarding best practices using the Rosetta modelling software. The authors also thank Koonin group members for helpful discussions. NDR, YIW, and EVK are supported by the Intramural Research Program of the National Institutes of Health (National Library of Medicine).

References

1. Zhan SH, Deverman BE, Chan YA. SARS-CoV-2 is well adapted for humans. What does this mean for re-emergence? BioRxiv. 2020.
2. van Dorp L, Richard D, Tan CC, Shaw LP, Acman M, Balloux F. No evidence for increased transmissibility from recurrent mutations in SARS-CoV-2. Nature communications. 2020;11(1):1-8.
3. Rochman ND, Wolf YI, Faure G, Mutz P, Zhang F, Koonin EV. Ongoing global and regional adaptive evolution of SARS-CoV-2. Proceedings of the National Academy of Sciences. 2021;118(29).
4. Rochman N, Wolf Y, Koonin EV. Evolution of human respiratory virus epidemics. F1000Research. 2021;10.
5. Saad-Roy CM, Wagner CE, Baker RE, Morris SE, Farrar J, Graham AL, et al. Immune life history, vaccination, and the dynamics of SARS-CoV-2 over the next 5 years. Science. 2020;370(6518):811-8.
6. Amanat F, Krammer F. SARS-CoV-2 vaccines: status report. Immunity. 2020;52(4):583-9.
7. Rochman N, Wolf Y, Koonin EV. Substantial impact of post-vaccination contacts on cumulative infections during viral epidemics. F1000Research. 2021;10.
8. Greaney AJ, Starr TN, Gilchuk P, Zost SJ, Binshtein E, Loes AN, et al. Complete mapping of mutations to the SARS-CoV-2 spike receptor-binding domain that escape antibody recognition. Cell host & microbe. 2021;29(1):44-57. e9.
9. Greaney AJ, Starr TN, Barnes CO, Weisblum Y, Schmidt F, Caskey M, et al. Mapping mutations to the SARS-CoV-2 RBD that escape binding by different classes of antibodies. Nature Communications. 2021;12(1):1-14.
10. Nelson G, Buzko O, Spilman PR, Niazi K, Rabizadeh S, Soon-Shiong PR. Molecular dynamic simulation reveals E484K mutation enhances spike RBD-ACE2 affinity and the combination of E484K, K417N and N501Y mutations (501Y. V2 variant) induces conformational change greater than N501Y mutant alone, potentially resulting in an escape mutant. BioRxiv. 2021.
11. Laffeber C, de Koning K, Kanaar R, Lebbink JH. Experimental evidence for enhanced receptor binding by rapidly spreading SARS-CoV-2 variants. Journal of Molecular Biology. 2021;433(15):167058.
12. Starr TN, Greaney AJ, Hilton SK, Ellis D, Crawford KH, Dingens AS, et al. Deep mutational scanning of SARS-CoV-2 receptor binding domain reveals constraints on folding and ACE2 binding. Cell. 2020;182(5):1295-310. e20.
13. Leaver-Fay A, Tyka M, Lewis SM, Lange OF, Thompson J, Jacak R, et al. ROSETTA3: an object-oriented software suite for the simulation and design of macromolecules. Methods in enzymology. 2011;487:545-74.
14. Li B, Deng A, Li K, Hu Y, Li Z, Xiong Q, et al. Viral infection and transmission in a large well-traced outbreak caused by the Delta SARS-CoV-2 variant. MedRxiv. 2021.
15. Duong D. Alpha, Beta, Delta, Gamma: What's important to know about SARS-CoV-2 variants of concern? : Can Med Assoc; 2021.
16. Lan J, Ge J, Yu J, Shan S, Zhou H, Fan S, et al. Structure of the SARS-CoV-2 spike receptor-binding domain bound to the ACE2 receptor. Nature. 2020;581(7807):215-20.
17. Jiang S, Hillyer C, Du L. Neutralizing antibodies against SARS-CoV-2 and other human coronaviruses. Trends in immunology. 2020;41(5):355-9.
18. Alford RF, Leaver-Fay A, Jeliazkov JR, O'Meara MJ, DiMaio FP, Park H, et al. The Rosetta all-atom energy function for macromolecular modeling and design. Journal of chemical theory and computation. 2017;13(6):3031-48.
19. Starr TN, Greaney AJ, Addetia A, Hannon WW, Choudhary MC, Dingens AS, et al. Prospective mapping of viral mutations that escape antibodies used to treat COVID-19. Science. 2021;371(6531):850-4.

764 20. Starr TN, Greaney AJ, Dingens AS, Bloom JD. Complete map of SARS-CoV-2 RBD mutations that
765 escape the monoclonal antibody LY-CoV555 and its cocktail with LY-CoV016. Cell Reports Medicine.
766 2021;2(4):100255.
767 21. Wang Z, Schmidt F, Weisblum Y, Muecksch F, Barnes CO, Finkin S, et al. mRNA vaccine-elicited
768 antibodies to SARS-CoV-2 and circulating variants. Nature. 2021;592(7855):616-22.
769 22. Greaney AJ, Loes AN, Crawford KH, Starr TN, Malone KD, Chu HY, et al. Comprehensive mapping
770 of mutations in the SARS-CoV-2 receptor-binding domain that affect recognition by polyclonal human
771 plasma antibodies. Cell host & microbe. 2021;29(3):463-76. e6.
772 23. Shu Y, McCauley J. GISAID: Global initiative on sharing all influenza data–from vision to reality.
773 Eurosurveillance. 2017;22(13):30494.
774 24. Zhang Q, Ju B, Ge J, Chan JF-W, Cheng L, Wang R, et al. Potent and protective IGHV3-53/3-66
775 public antibodies and their shared escape mutant on the spike of SARS-CoV-2. Nature communications.
776 2021;12(1):1-12.
777 25. Alenquer M, Ferreira F, Lousa D, Valerio M, Medina-Lopes M, Bergman M-L, et al. Amino acids
778 484 and 494 of SARS-CoV-2 spike are hotspots of immune evasion affecting antibody but not ACE2
779 binding. bioRxiv. 2021.
780 26. Breen MS, Kemena C, Vlasov PK, Notredame C, Kondrashov FA. Epistasis as the primary factor in
781 molecular evolution. Nature. 2012;490(7421):535-8.
782 27. Sakai W, Swisher EM, Karlan BY, Agarwal MK, Higgins J, Friedman C, et al. Secondary mutations
783 as a mechanism of cisplatin resistance in BRCA2-mutated cancers. Nature. 2008;451(7182):1116-20.
784 28. Levin BR, Perrot V, Walker N. Compensatory mutations, antibiotic resistance and the population
785 genetics of adaptive evolution in bacteria. Genetics. 2000;154(3):985-97.
786 29. Rochman ND, Wolf YI, Koonin EV. Deep phylogeny of cancer drivers and compensatory
787 mutations. Communications biology. 2020;3(1):1-11.
788 30. Kupferschmidt K. Where did 'weird'Omicron come from? : American Association for the
789 Advancement of Science; 2021.
790 31. Wilhelm A, Widera M, Grikscheit K, Toptan T, Schenk B, Pallas C, et al. Reduced Neutralization of
791 SARS-CoV-2 Omicron Variant by Vaccine Sera and monoclonal antibodies. medRxiv. 2021.
792 32. Gruell H, Vanshylla K, Tober-Lau P, Hillus D, Schommers P, Lehmann C, et al. mRNA booster
793 immunization elicits potent neutralizing serum activity against the SARS-CoV-2 Omicron variant.
794 medRxiv. 2021.
795 33. Zhang Y, Zhang J, Chen Y, Luo B, Yuan Y, Huang F, et al. The ORF8 protein of SARS-CoV-2
796 mediates immune evasion through potently downregulating MHC-I. BioRxiv. 2020.
797 34. Zinzula L. Lost in deletion: The enigmatic ORF8 protein of SARS-CoV-2. Biochemical and
798 biophysical research communications. 2021;538:116-24.
799 35. Garushyants SK, Rogozin IB, Koonin EV. Template switching and duplications in SARS-CoV-2
800 genomes give rise to insertion variants that merit monitoring. Communications Biology. 2021;4(1):1-9.
801 36. Zhang J, Cai Y, Xiao T, Lu J, Peng H, Sterling SM, et al. Structural impact on SARS-CoV-2 spike
802 protein by D614G substitution. Science. 2021;372(6541):525-30.
803 37. Hurlburt NK, Seydoux E, Wan Y-H, Edara VV, Stuart AB, Feng J, et al. Structural basis for potent
804 neutralization of SARS-CoV-2 and role of antibody affinity maturation. Nature communications.
805 2020;11(1):1-7.
806 38. Seydoux E, Homad LJ, MacCamy AJ, Parks KR, Hurlburt NK, Jennewein MF, et al. Analysis of a
807 SARS-CoV-2-infected individual reveals development of potent neutralizing antibodies with limited
808 somatic mutation. Immunity. 2020;53(1):98-105. e5.
809 39. Voss WN, Hou YJ, Johnson NV, Delidakis G, Kim JE, Javanmardi K, et al. Prevalent, protective, and
810 convergent IgG recognition of SARS-CoV-2 non-RBD spike epitopes. Science. 2021;372(6546):1108-12.

811 40. Tyka MD, Keedy DA, André I, DiMaio F, Song Y, Richardson DC, et al. Alternate states of proteins
812 revealed by detailed energy landscape mapping. Journal of molecular biology. 2011;405(2):607-18.
813 41. Fleishman SJ, Leaver-Fay A, Corn JE, Strauch E-M, Khare SD, Koga N, et al. RosettaScripts: a
814 scripting language interface to the Rosetta macromolecular modeling suite. PloS one. 2011;6(6):e20161.
815 42. Tovchigrechko A, Vakser IA. How common is the funnel-like energy landscape in protein-protein
816 interactions? Protein science. 2001;10(8):1572-83.
817 43. Grünberg R, Nilges M, Leckner J. Flexibility and conformational entropy in protein-protein
818 binding. Structure. 2006;14(4):683-93.
819 44. Barlow KA, Ó Conchúir S, Thompson S, Suresh P, Lucas JE, Heinonen M, et al. Flex ddG: Rosetta
820 ensemble-based estimation of changes in protein–protein binding affinity upon mutation. The Journal of
821 Physical Chemistry B. 2018;122(21):5389-99.
822 45. Xue T, Wu W, Guo N, Wu C, Huang J, Lai L, et al. Single point mutations can potentially enhance
823 infectivity of SARS-CoV-2 revealed by in silico affinity maturation and SPR assay. RSC Advances.
824 2021;11(24):14737-45.
825 46. Riahi S, Lee JH, Wei S, Cost R, Masiero A, Prades C, et al. Application of an integrated
826 computational antibody engineering platform to design SARS-CoV-2 neutralizers. bioRxiv. 2021.
827 47. Desautels T, Zemla A, Lau E, Franco M, Faissol D. Rapid in silico design of antibodies targeting
828 SARS-CoV-2 using machine learning and supercomputing. BioRxiv. 2020.
829 48. Epistasis at the SARS-CoV-2 RBD Interface and the Propitiously Boring Implications for Vaccine
830 Escape [Data set] [Internet]. 2021.

831

832

833

834 ## Figure legends

835 **Figure 1. Landscape of Vaccine Escape Mutants for the WT RBD**

836 **A.** Cartoon depicting unique conformational changes to the RBD (blue) in complex with
837 ACE2 (orange) and the NAb (green) associated with the same mutation. **B.** Cartoon
838 depicting the landscape of vaccine escape mutations (the plane of receptor cost vs
839 antibody cost). **C.** Landscape of vaccine escape mutations for the WT RBD. Circles with
840 a black outline are NAb escape candidates. Color indicates propensity for escape as
841 measured by $\Delta\Delta G$.

842

843 **Figure 2. Dominant Trends in Circulating RBD Mutations**

844 **A.** Region-normalized global prevalence of the top 10 most common combinations of
845 RBD mutations over time. Lines are solid up to peak prevalence and dashed afterwards.
846 Shading indicates confidence intervals. **B.** Structural comparison of the complexes of
847 ACE2 and NAb with RBD for WT, Delta, Gamma, and Omicron variants. *Top*: WT
848 footprints including the residues with an interaction within 4A of the partner. *Bottom:*
849 Visualization of the Delta, Gamma, and Omicron variant interfaces. Mutations are
850 labeled and represented as sticks. WT structures are superimposed for the RBD of
851 each variant: WT, orange; variant, olive **C.** Interface RMSD for ACE2 and NAb
852 complexes relative to an arbitrary WT conformation (over spike protein sites 403-
853 406,408-409,414-417,419-421,439,445-447,449,453,455-461,473-478,480,484-506).
854 Asterisks denote p-values less than 0.02 for a Wilcoxon Rank Sum Test. **D.** CMDS
855 applied to the pairwise RMSDs among all RBD-ACE2 and RBD-NAb complexes. 2D
856 visualizations of 3D projections are displayed (see Figure S2 for 3D).

857

858 **Figure 3. Epistasis within the RBD.**

859 **A.** Cartoon illustrating additive and non-additive (epistatic) interactions between
860 mutations. From top to bottom: additive, escape-neutral, escape-minimizing, and
861 escape-exacerbating. *Mi, Mj, Mij* denote the effects of the single and double mutants. **B.**
862 *Top:* Landscape of vaccine escape mutations for the variant RBDs. Coloring, as in
863 Figure 1C, indicates propensity for escape as measured by $\Delta\Delta G$. Circles with a black

outline denote NAb escape candidates. Dashed lines highlight differences among variants. *Bottom:* Landscape of vaccine escape mutations for the WT RBD. Black points are candidates for both WT and variant; gray points are not candidates for either WT or variant; green points are only candidates for WT; red points are only candidates for the variant.

Figure 4. Landscape of Epistatic Effects Supporting Enhanced Vaccine Escape
Non-additive escape-exacerbating motifs in Delta (top), Gamma (middle), and Omicron (bottom) variants. The size of each letter corresponds to the increased likelihood of vaccine escape for the substitution in the variant relative to the WT. *Inset*: Total score change ($[S_M^C - S_{WT}^C]_{NAb}$) induced by mutation in the Gamma (black) and Omicron variants (red) vs the WT (identity line overlaid). The minimum value (less 1) is subtracted from each distribution for normalization (see Figure S5 for more).

877 **Table 1: Receptor-binding and antibody-binding interface footprints in the RBD**

WT RBD-ACE2 Footprint	403, 405, 417, 445-447, 449, 453, 455-456, 473-478, 484-491, 493-498, 500-506
Delta RBD-ACE2 Footprint	Same as WT
Gamma RBD-ACE2 Footprint	WT + 404, 406, 408, 439, 499 - 484
Omicron RBD-ACE2 Footprint	WT + 404, 439, 499 - 445, 484, 491
WT RBD-NAb Footprint	403-406, 409, 414-417, 419-421, 446-447, 449, 453, 455-461, 473-478, 484-498, 500-506
Delta RBD-NAb Footprint	Same as WT
Gamma RBD-NAb Footprint	WT + 408, 480
Omicron RBD-NAb Footprint	WT - 446

878

879

880 **Table 2: Numbers of antibody-escape candidates**

881

	Total		WT not Variant	Variant not WT	Difference
WT	241	Δ	15(13)	6(2)	-9(-11)
Delta	232	Γ	32(28)	86(66)	54(38)
Gamma	295	O	67(59)	75(48)	8(-11)
Omicron	249				

882

883 Values in parentheses are tabulated mutations with $[S_M^C - S_{WT}^C]_{ACE2} < 13$, for both the
884 WT and variant.

885

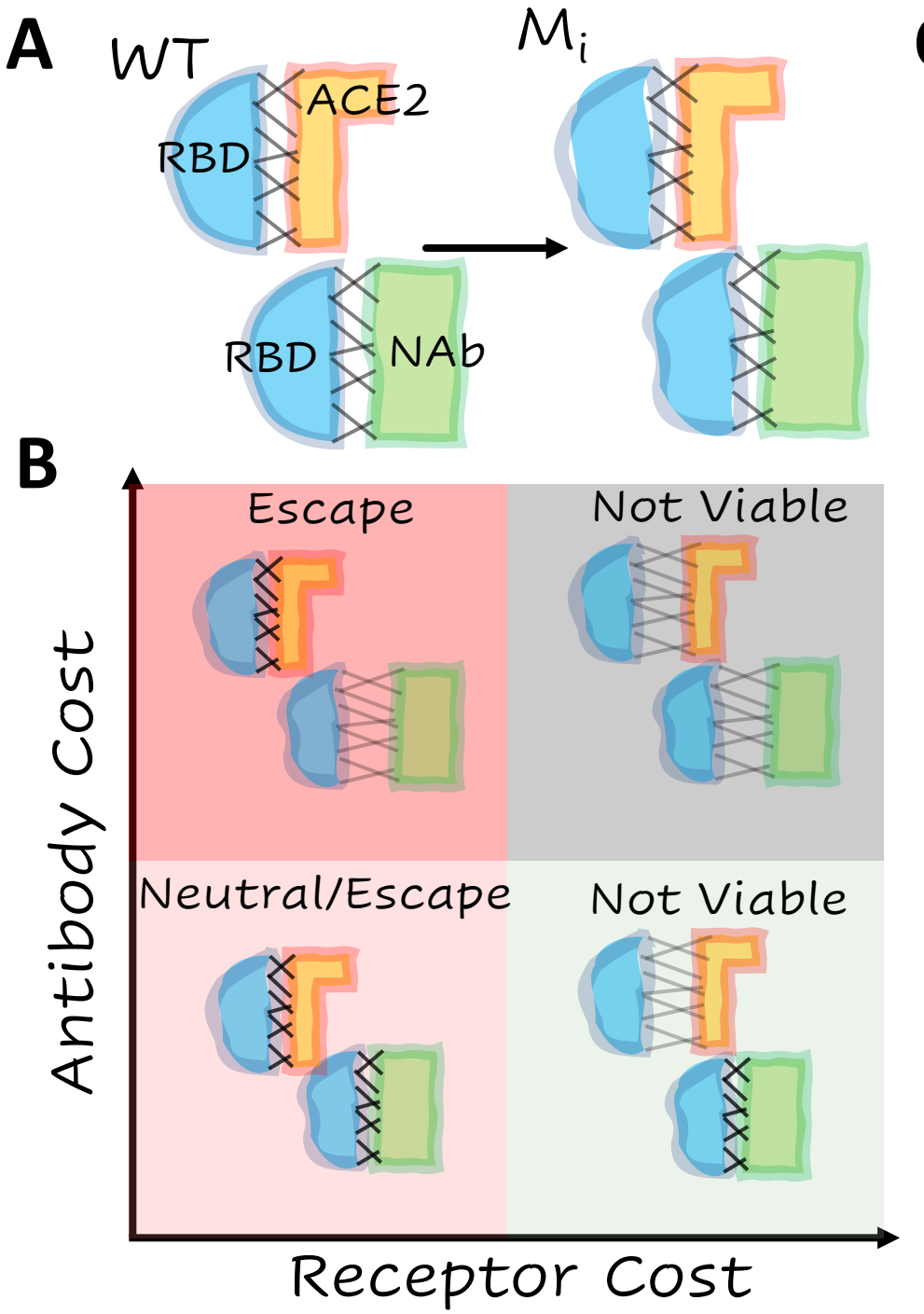
A
WT
ACE2
RBD
RBD
NAb
M_i
B
Escape
Not Viable
Neutral/Escape
Not Viable
Antibody Cost
Receptor Cost

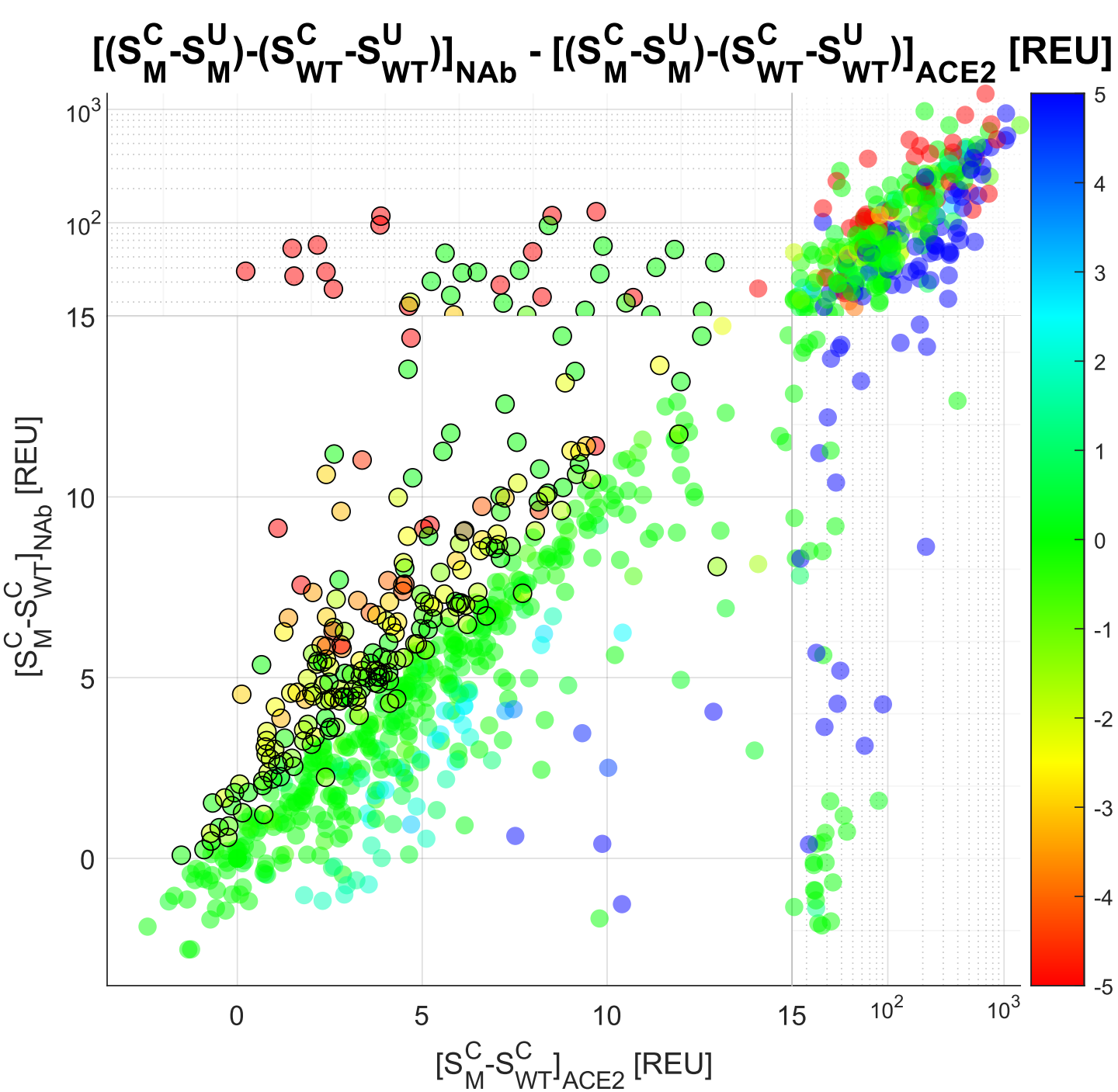
C
$[(S_M^C-S_M^U)-(S_{WT}^C-S_{WT}^U)]_{NAb} - [(S_M^C-S_M^U)-(S_{WT}^C-S_{WT}^U)]_{ACE2}$ [REU]
$[S_M^C-S_{WT}^C]_{NAb}$ [REU]
$[S_M^C-S_{WT}^C]_{ACE2}$ [REU]
10^3
10^2
15
10
5
0
0
5
10
15
10^2
10^3
5
4
3
2
1
0
-1
-2
-3
-4
-5

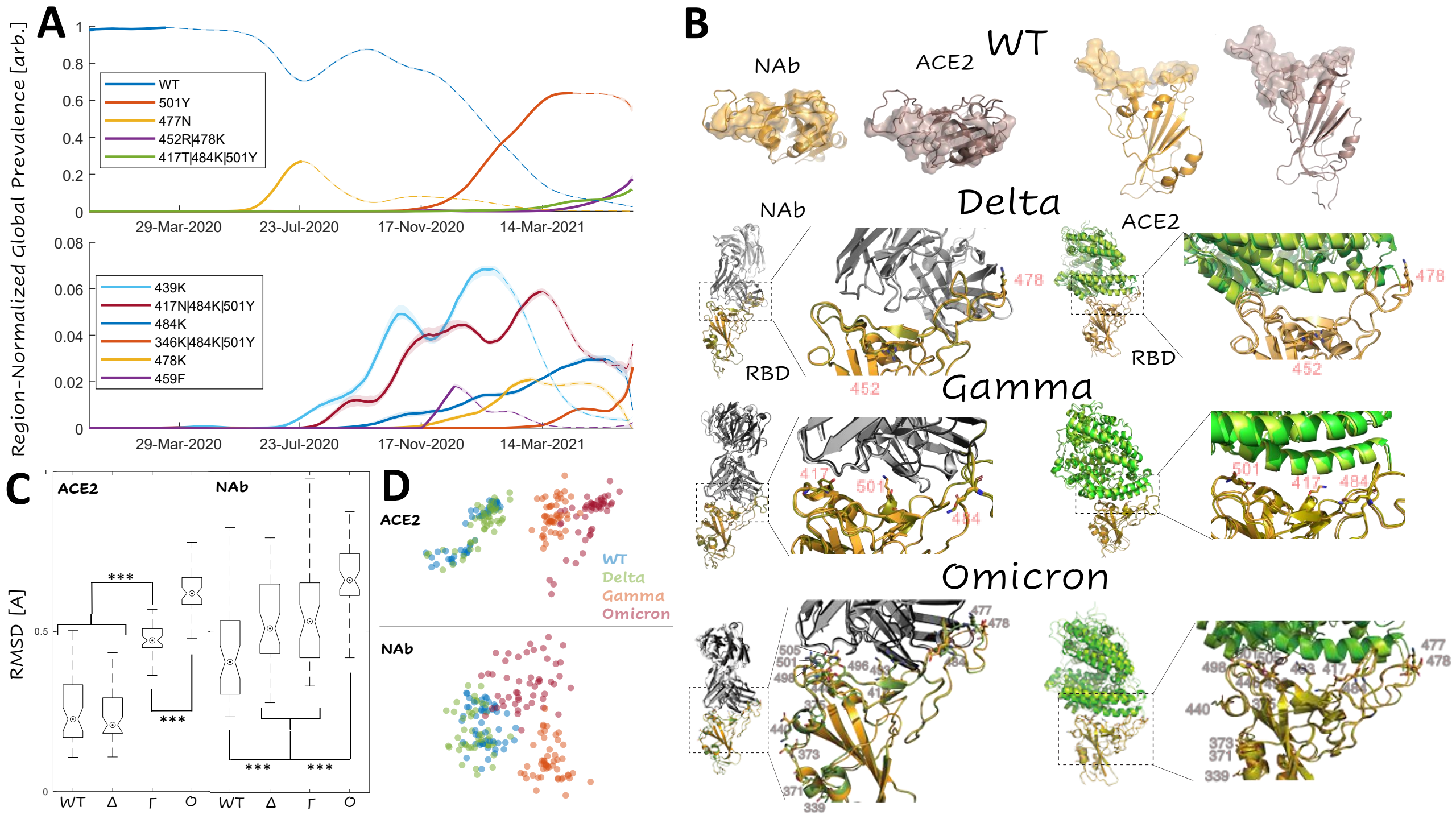
A
Region-Normalized Global Prevalence [arb.]
WT
501Y
477N
452R|478K
417T|484K|501Y
439K
417N|484K|501Y
484K
346K|484K|501Y
478K
459F
29-Mar-2020
23-Jul-2020
17-Nov-2020
14-Mar-2021
B
WT
NAb
ACE2
Delta
RBD
478
452
Gamma
417
501
484
Omicron
477
505
496
498
440
373
371
339
C
ACE2
NAb
RMSD [A]
***
WT
Δ
Γ
O
D
ACE2
NAb
WT
Delta
Gamma
Omicron

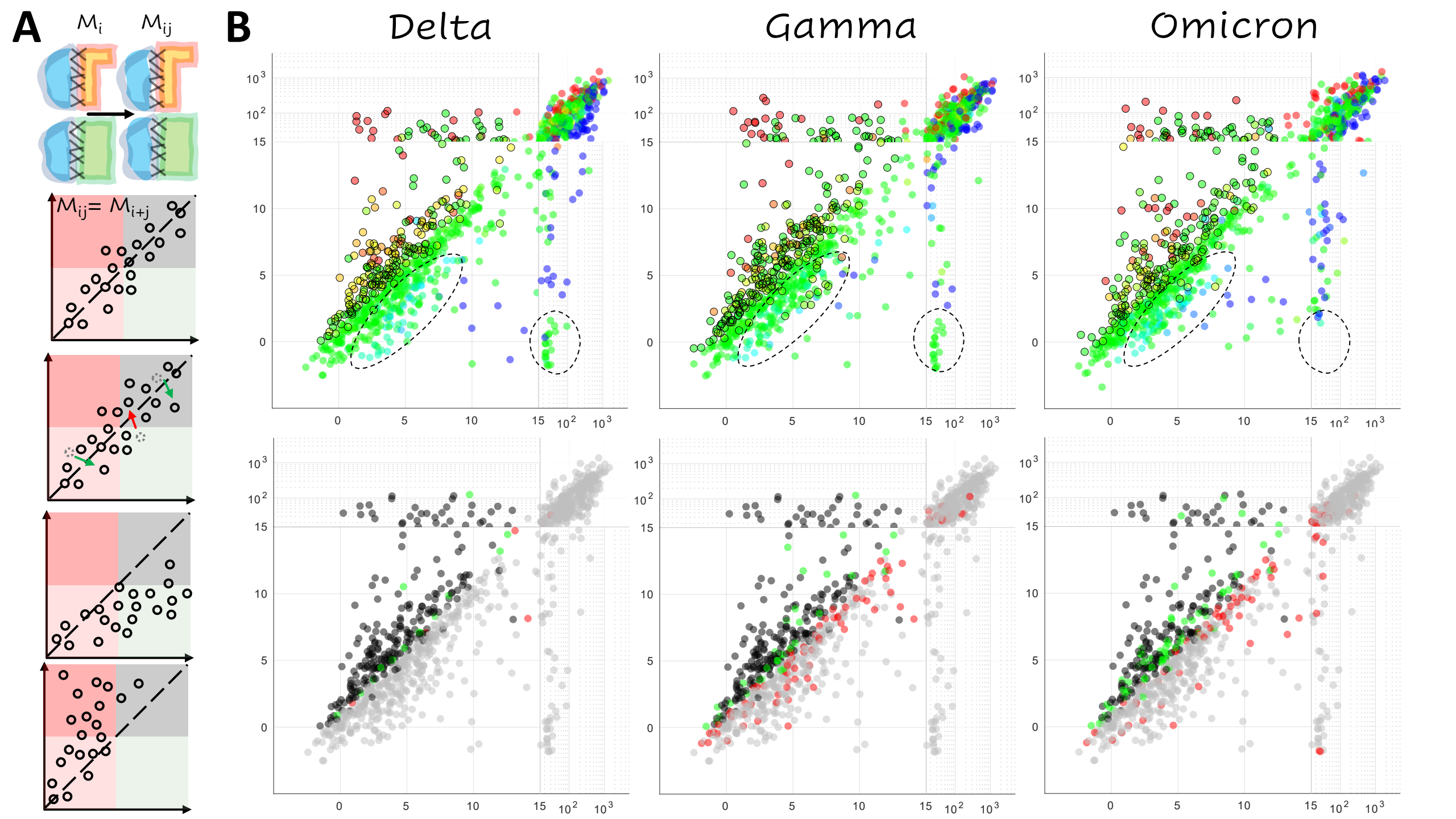
A
M_i
M_{ij}
$M_{ij} = M_{i+j}$
B
Delta
Gamma
Omicron

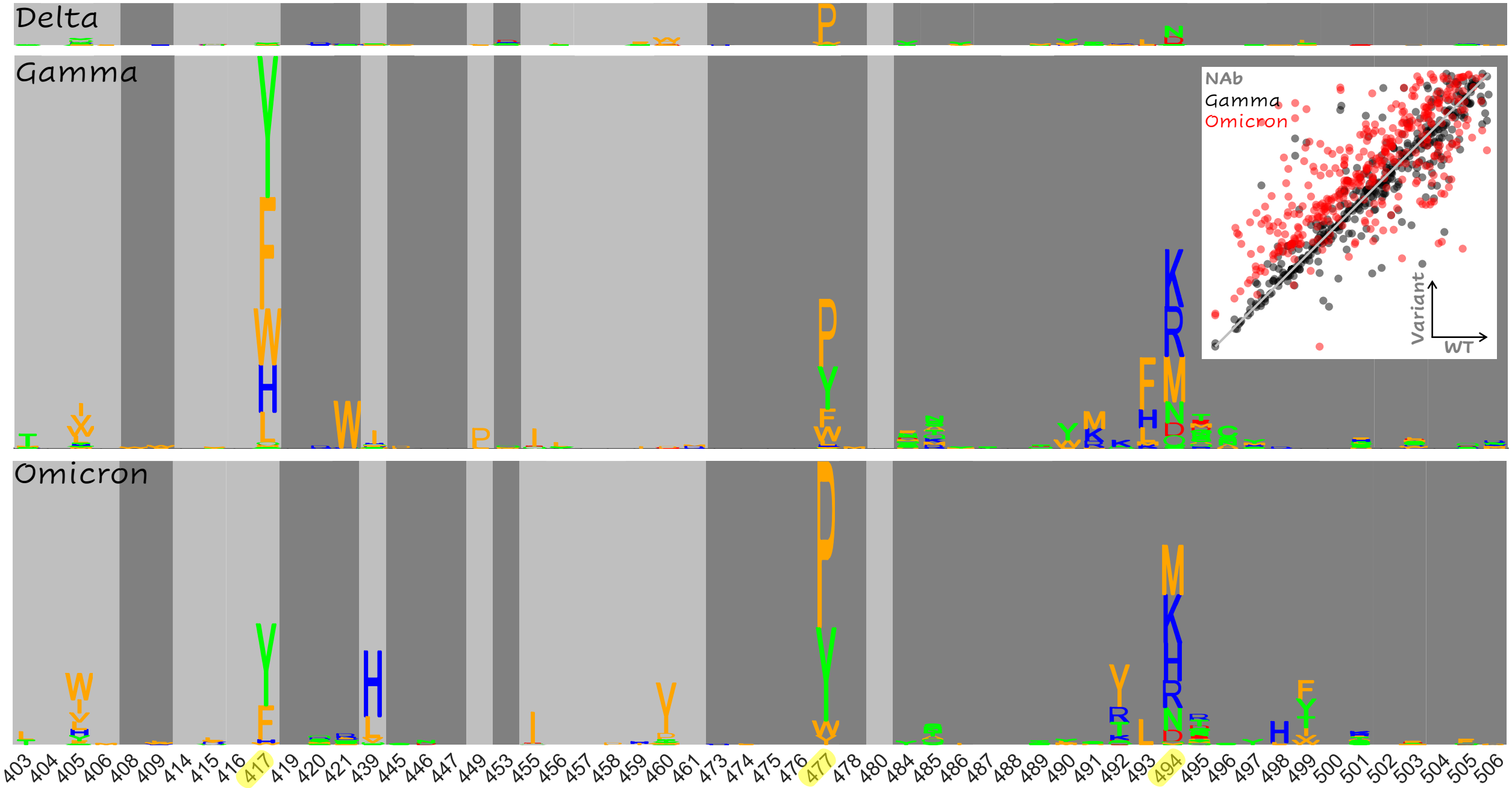
Delta
Gamma
Omicron
NAb
Gamma
Omicron
Variant
WT
403 404 405 406 408 409 414 415 416 417 419 420 421 439 445 446 447 449 453 455 456 457 458 459 460 461 473 474 475 476 477 478 480 484 485 486 487 488 489 490 491 492 493 494 495 496 497 498 499 500 501 502 503 504 505 506